

Heterometallic gold(I)–thallium(I) compounds with crown thioether†‡

Cite this: *Dalton Trans.*, 2013, **42**, 11559Alexander J. Blake,^a Rocío Donamaría,^b Eduardo J. Fernández,^b Tania Lasanta,^b Vito Lippolis,^{*c} José M. López-de-Luzuriaga,^{*b} Elena Manso,^b Miguel Monge^b and M. Elena Olmos^b

The polymeric Au/Tl compounds $[\{Au(C_6X_5)_2\}Tl]_n$ (X = Cl, F) react with the crown thioethers 1,4,7-trithia-cyclononane ([9]aneS₃), 1,5,8,11-tetrathiacyclotetradecane ([14]aneS₄), and 1,4,7,10,13,16,19,22-octathia-cyclotetrasolane ([24]aneS₈) in an appropriate molar ratio to afford $[\{Au(C_6X_5)_2\}Tl(L)]_2$ [L = [9]aneS₃, X = Cl (**1**), F (**4**); L = [14]aneS₄, X = Cl (**2**), F (**5**)], $[\{Au(C_6Cl_5)_2\}_2Tl_2\{[24]aneS_8\}_n$ (**3**) or $[\{Au(C_6F_5)_2\}_2Tl_2\{[24]aneS_8\}]$ (**6**). X-ray diffraction studies of **3**, **4** and **6** reveal polymeric (**3**) or tetranuclear (**4**, **6**) structures formed via Tl–S bonds and Au...Tl or Au...Tl and Au...Au contacts. All the complexes are luminescent in the solid state, but not in solution, where the metal–metal interactions, which are responsible for the luminescence, are no longer present. DFT calculations on representative model systems of complexes **3**, **4** and **6** have also been carried out in order to determine the origin of the electronic transitions responsible for their optical properties.

Received 22nd May 2013,

Accepted 15th June 2013

DOI: 10.1039/c3dt51334c

www.rsc.org/dalton

Introduction

The chemistry of heteropolynuclear extended supramolecular systems built by secondary interactions has attracted physicists' and chemists' interest in recent years. This is mainly due to the particular characteristics of the chemical bonding in these systems and to the physical and chemical properties associated with them.¹ As is well known, aurophilic interactions, which are comparable in strength to hydrogen bonds,² are the most widely studied nonbonding contacts between closed-shell metal ions. Nevertheless, over the past few years, complexes with metallophilic interactions between gold(I) centres and other closed-shell metal atoms (Au(I)···M) have attracted renewed attention due to their theoretical aspects,³ photophysical properties⁴ and potential applications.⁵ In particular, the luminescence observed in these compounds seems to be closely related to the presence of metal···metal interactions, which have in many cases been implicated in these

optical properties.⁶ Besides, this luminescence strongly depends on the structural arrangement of the metals, on their environment and on the nature of the ligands present in the complex.⁷

One of the synthetic methods usually employed in our laboratory for the preparation of heteropolynuclear extended systems is the acid–base strategy, consisting of the treatment of electron-rich neutral molecules or anions with Lewis acids. These reactions lead to an enormous variety of structural arrangements, which range from discrete molecules to extended structures of varying dimensionality.⁸ In particular, we have extensively employed bis(perhalophenyl)aurate(I) salts as basic precursors and closed-shell metal ions such as Ag(I)⁹ or Tl(I)^{6,7} as the acidic ones. For example, treatment of NBu₄[Au(C₆X₅)₂] (X = Cl, F) with TlPF₆ affords the compound $[\{Au(C_6X_5)_2\}Tl]_n$, featuring one-dimensional polymeric chains with alternating gold and thallium atoms^{5a,7c,10} which further react with different electron donor molecules that may interact with the thallium centres. In previous work, we have reported that the changing of the halogens in the bis(perhalophenyl)aurate(I) precursor modifies the donor properties of the aurate(I) fragment and, consequently, different structural and photophysical properties can be obtained.^{7a,10} Similarly, the nature and characteristics of the donor species that bind the thallium atoms are also of crucial importance in the structural disposition of the resulting materials. In fact, a “butterfly” disposition of metals has only been observed when ketones are added as ligands.¹¹ Many examples of Au/Tl compounds with N, O or Se-donor ligands^{7a,11,12} or even metallic fragments^{10a}

^aSchool of Chemistry, The University of Nottingham, University Park, Nottingham NG7-2RD, UK

^bDepartamento de Química, Universidad de La Rioja, Centro de Investigación en Síntesis Química (CISQ), Complejo Científico-Tecnológico, 26004-Logroño, Spain. E-mail: josemaria.lopez@unirioja.es

^cDipartimento di Scienze Chimiche e Geologiche, Università degli Studi di Cagliari, S.S. 554 Bivio per Sestu, 09042 Monserrato (CA), Italy. E-mail: lippolis@unica.it

†Dedicated to Professor A. Laguna on the occasion of his 65th birthday.

‡Electronic supplementary information (ESI) available. CCDC 935229–935231. For ESI and crystallographic data in CIF or other electronic format see DOI: 10.1039/c3dt51334c

bonded to thallium have been reported by our group over the last few years. However, only a couple of Au/Tl derivatives with Tl-S bonds are known (from the 1980s), both of them containing the asymmetric C,S-ligand $[\text{CH}_2\text{P}(\text{S})\text{Ph}_2]^-$.¹³

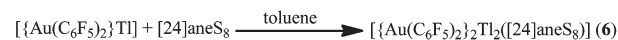
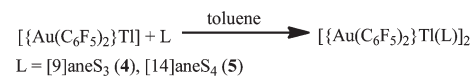
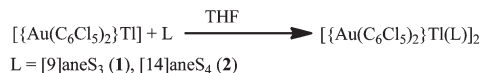
On the other hand, crown thioethers with different numbers of S-donor atoms have been employed for the synthesis of a large number of coordination compounds with a great variety of metal centres.¹⁴ These macrocycles can form stable, inert complexes with a wide range of transition metal ions, sometimes forcing the metal centre to adopt unusual coordination geometries and/or oxidation states.¹⁵ The majority of these studies are focused on the chemistry of 1,4,7-trithiacyclononane ([9]aneS₃), 1,4,7,10-tetrathiacyclododecane ([12]aneS₄), 1,5,9,13-tetrathiacyclohexadecane ([16]aneS₄), and 1,4,7,10,13,16-hexathiacyclooctadecane ([18]aneS₆), while the coordination of larger rings, such as 1,4,7,10,13,16,19,22-octathiacyclotetracosane ([24]aneS₈) or 1,4,8,11,15,18,22,25-octathiacyclooctacosane ([28]aneS₈), is less studied. Furthermore, a systematic examination of the coordination chemistry of p-block metal ions¹⁶ and d¹⁰ transition metal ions¹⁷ with thioether crowns still remains an open area of investigation. Specifically, there are only three examples of structurally characterized thallium(i) complexes with crown thioethers, namely, $[\text{Tl}(\text{[9]aneS}_3)]\text{PF}_6$,^{16e} $[\text{Tl}(\text{[18]aneS}_6)]\text{PF}_6$,¹⁸ and $[\text{Tl}(\text{[24]aneS}_8)]\text{PF}_6$.^{16d} In $[\text{Tl}(\text{[9]aneS}_3)]\text{PF}_6$ the trithia macrocycle is bound facially to the metal ion and a thioether donor from an adjacent complex cation makes a longer contact, thus linking $[\text{Tl}(\text{[9]aneS}_3)]^+$ cations into infinite helices. A similar situation is observed in $[\text{Tl}(\text{[18]aneS}_6)]\text{PF}_6$. In $[\text{Tl}(\text{[24]aneS}_8)]\text{PF}_6$, each Tl⁺ ion is sandwiched between two symmetry-related halves of two [24]aneS₈ molecules within an infinite one-dimensional sinusoidal polymer.

Taking the above into account, we decided to study the reactivity of the crown thioethers [9]aneS₃, [14]aneS₄ and [28]aneS₈ with the hetero-dimetallc compounds $[\{\text{Au}(\text{C}_6\text{X}_5)_2\}\text{Tl}]_n$ (X = Cl, F) and thereby determine whether the number of sulphur atoms present in the S-donor ligands modifies the structural disposition of the two metal centres in the starting polymeric material, since a behaviour as a terminal or a bridging ligand of the macrocyclic systems is expected to depend on the number of S-donor centres and the size of the ring cavity. Additionally, the modification of the halogen present in the aryl groups bonded to gold may also influence the acidic properties of the thallium centres. Both factors may therefore result in different coordination environments at Tl⁺ and give rise to different arrangements of metals, which may modify the number and strength for the unsupported Au...Tl interactions and, consequently, their optical properties.

Results and discussion

Synthesis and characterization

The heterometallic complexes $[\{\text{Au}(\text{C}_6\text{Cl}_5)_2\}\text{Tl}(\text{L})_2]$ [L = [9]aneS₃ (1), [14]aneS₄ (2)], were obtained by reaction of the polymetallic chain compound $[\{\text{Au}(\text{C}_6\text{Cl}_5)_2\}\text{Tl}]_n$ with equimolecular



Scheme 1

amounts of the corresponding thioether crown ligand in tetrahydrofuran. As expected, the higher number of sulphur atoms in [24]aneS₈ leads to a compound with a different ratio of metals and ligands, $[\{\text{Au}(\text{C}_6\text{Cl}_5)_2\}_2\text{Tl}_2([\text{24]aneS}_8)]_n$ (3), which was obtained by reaction of the same polymetallic chain $[\{\text{Au}(\text{C}_6\text{Cl}_5)_2\}\text{Tl}]_n$ with [24]aneS₈ in a 2:1 molar ratio using tetrahydrofuran as a solvent (Scheme 1). Although the synthesis of complexes 1–3 can also be carried out in toluene, the use of THF leads to higher yields. The substitution of the chlorine atoms in the aryl groups bonded to gold by fluorine does not seem to affect the stoichiometry of the resulting compounds, and, thus, similarly, the pentafluorophenyl derivatives $[\{\text{Au}(\text{C}_6\text{F}_5)_2\}\text{Tl}(\text{L})_2]$ [L = [9]aneS₃ (4), [14]aneS₄ (5)] and $[\{\text{Au}(\text{C}_6\text{F}_5)_2\}_2\text{Tl}_2([\text{24]aneS}_8)]$ (6) were obtained by following the same procedure as for the synthesis of 1–3 using the same reaction molar ratios of the starting products, but using $[\{\text{Au}(\text{C}_6\text{F}_5)_2\}\text{Tl}]_n$ as a starting material and toluene as a solvent (see Scheme 1). In the case of complexes 4–6, their synthesis is also possible in tetrahydrofuran, but unlike the results in the preparation of 1–3, its employment as a solvent gave rise to the complexes in lower yield.

All the complexes are stable to air and moisture for long periods. They are insoluble in dichloromethane, acetonitrile and diethyl ether, but soluble in O-donor solvents such as tetrahydrofuran or acetone.

Their elemental analyses and spectroscopic data are in accordance with the proposed stoichiometries (see the Experimental section). Their IR spectra in nujol display, among others, absorptions arising from the C₆F₅¹⁹ and C₆Cl₅²⁰ groups bonded to gold(i) at approximately 1500, 950 and 780 cm⁻¹ or about 834 and 614 cm⁻¹, respectively. The presence of the $[\text{Au}(\text{C}_6\text{F}_5)_2]^-$ fragment in 4–6 is evident in their ¹⁹F NMR spectra, which resemble that of the precursor complex $\text{NBu}_4[\text{Au}(\text{C}_6\text{F}_5)_2]$, and seem to indicate that a dissociative process giving rise to aurate(i) anions and thallium(i) cations takes place in solution. Regarding the ¹H NMR spectra of complexes 1–6 in [D₈]tetrahydrofuran, they all show the resonances corresponding to the crown thioethers at similar chemical shifts to those found for the free ligands. Therefore, the coordination of the macrocyclic ligands to thallium does not significantly affect the position of the resonances observed in their ¹H NMR spectra, nor does the dissociative process

affect the S-donor molecules. Thus, the ^1H NMR spectra of **2** and **5** display three signals at 2.01 (q, 4H, S-CH₂-CH₂-CH₂-S), 2.73 (t, 8H, S-CH₂-CH₂-CH₂-S) and 2.85 ppm (s, 8H, S-CH₂-CH₂-S), while in the ^1H NMR spectra of the rest of the products a unique singlet at 3.20 (**1** and **4**) or at 2.92 ppm (**3** and **6**) is observed. The molar conductivity measurements of solutions of the complexes in acetone are of special relevance, since they are consistent with an ionic formulation as 1 : 1 electrolytes for complexes **1**, **2**, **4** and **5**, and as 2 : 1 electrolytes for complexes **3** and **6**. This suggests that the units $[\text{Au}(\text{C}_6\text{X}_5)_2]^-$ and $[\text{Tl}(\text{L})]^+$ (**1**, **2**, **4** and **5**) or $[\text{Tl}_2(\text{L})]^{2+}$ (**3** and **6**) are the species present in solution. Finally, in their mass spectra (MALDI-) a peak due to the unit $[\{\text{Au}(\text{C}_6\text{X}_5)_2\}_2\text{Tl}]^-$ at $m/z = 1595$ (**1**-**3**) or 1266 (**4**-**6**), as well as a signal corresponding to $[\text{Au}(\text{C}_6\text{X}_5)_2]^-$ at $m/z = 695$ (**1**-**3**) or 531 (**4**-**6**) are observed, the latter appearing as a parent peak. In the MALDI+ mass spectra peaks due to the fragments $[\text{Tl}(\text{L})]^+$ at $m/z = 385$ (**1**, **4**), 473 (**2**, **5**) or 685 (**3**, **6**) are observed with the experimental isotopic distributions in agreement with the theoretical ones.

X-ray structural determination of derivatives **3**, **4** and **6**

Single crystals suitable for X-ray diffraction studies of complexes **3**, **4** and **6** were obtained by slow diffusion of *n*-hexane into saturated solutions of the complexes in tetrahydrofuran. Although they all contain similar structural motifs: $[\text{Au}(\text{C}_6\text{X}_5)_2]^-$ fragments linked to Tl(I) centres through Au...Tl contacts, and each thallium connected to the macrocyclic ligand through the sulphur atoms, the three crystal structures are different. This is due to the behaviour of the crown thioether as a terminal or as a bridging ligand as well as to the presence or absence of auriphilic interactions. Therefore, in the cases of complexes **3** and **6**, where the ligand [24]aneS₈ coordinates two Tl(I) centres, an Au-Tl-L-Tl-Au disposition is observed (Fig. 1). However, while the crystals of **6** contain discrete tetranuclear $[\{\text{Au}(\text{C}_6\text{F}_5)_2\}_2\text{Tl}_2(\text{[24]aneS}_8)]$ molecules, the solid state structure of **3** displays polymeric chains as a result of unsupported auriphilic contacts between the Au(I) centres (see Fig. 2). In contrast, in **4** the crown thioether [9]aneS₃ acts as a terminal ligand and Au...Au interactions are also observed, which results in tetranuclear discrete molecules

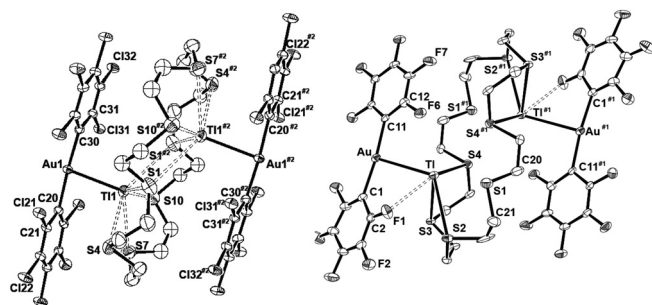


Fig. 1 Part of the crystal structure of compound **3** (left) and molecular structure of compound **6** (right) with the labelling scheme for the atom positions. Hydrogen atoms are omitted for clarity and ellipsoids are drawn at the 30% level. #1 $-x + 2, -y + 2, -z + 1$ #2 $-x, -y + 1, -z$.

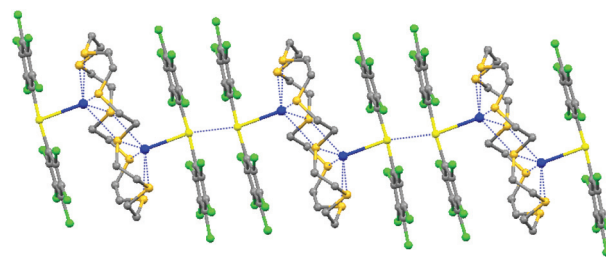


Fig. 2 Partial view of polymeric heterobimetallic chains in compound **3**. Hydrogen atoms are omitted for clarity. Colour code: gold: yellow; thallium: blue; sulphur: orange; carbon: grey; chlorine: green.

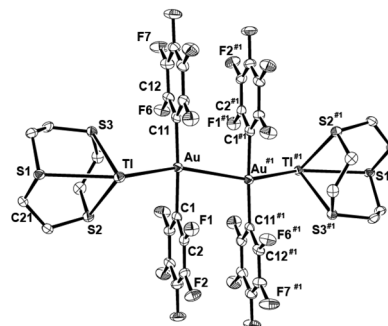


Fig. 3 Molecular structure of compound **4** with the labelling scheme for the atom positions. Hydrogen atoms are omitted for clarity and ellipsoids are drawn at the 30% level. #1 $-x + 1, -y + 1, -z$.

with a L-Tl-Au-Au-Tl-L disposition, *i.e.*, the crystal structure and L/Tl ratio differ from those in **3** and **6** (Fig. 3).

In view of these crystal structures, we can confirm our hypothesis about the influence of the nature of the ligands at thallium on the metal ion arrangements in the final products, since the vast majority of Au/Tl complexes with Au...Tl contacts display polymeric networks with alternating gold and thallium atoms,^{5b,c,6a,7,10,13,21} even with bulky N- or O-donor ligands at thallium.^{6a} A polymeric disposition similar to that found in **3** has only been previously observed in the complex $[\text{Tl}(\text{bipy})]_2[\text{Au}(\text{C}_6\text{F}_5)_2]_2$ which contains bridging 4,4'-bipyridine ligands and Au...Au contacts, while the pentachlorophenyl derivative displays the usual Au-Tl-Au-Tl disposition of metals and the bipyridine ligands bridging adjacent poly-metallic chains.^{7a} The electronic effects associated with the modification of the halogens in the aryl groups could be responsible for the formation of a tetranuclear molecule in **6** instead of a polymeric chain through Au...Au contacts, as in complex **3**, since the smaller fluorine atoms in **6** should favour the presence of auriphilic interactions in the latter if steric effects were the dominant ones. Thus, the structure of **6** represents a very unusual arrangement only found in the $[\{\text{Au}(\text{C}_6\text{Cl}_5)_2\text{Tl}(\text{toluene})\}_2(\text{dioxane})]$ complex, where the dioxane molecule bridges both thallium centres and no auriphilic contacts are observed (the Au...Au separation is 3.876 Å).²²

On the other hand, complex **4** represents the first example of a Au/Tl discrete molecule with a L-Tl-Au-Au-Tl-L sequence of ligands and metals.

In all the structures the gold centres are linearly coordinated to the *ipso* carbon atoms of the perhalophenyl ligands, with normal Au–C bond distances between 2.046(7) and 2.056(7) Å, and with a maximum deviation from linearity of 6.3° seen in **6**. Additionally, the crystal structures of both **3** and **4**, which contain different aryl groups and macrocycles, display aurophilic interactions of 3.3497(11) and 3.3294(6) Å, respectively (Tables 2 and 3). These Au–Au distances are shorter than those in [Tl(bipy)]₂[Au(C₆F₅)₂]₂ (3.4092(3) Å),^{7a} or in other related polymeric Au/Tl complexes,^{5b,c,6a,7,10,13,21} all of them showing Au–Au separations longer than 3.5 Å (3.825 Å in **6**), thereby excluding the possibility of significant interaction between gold atoms.

Although they are inequivalent, the Au–Tl distances are consistent with the presence of metallophilic interactions in the three structures. Therefore, the pentachlorophenyl complex **3**, which shows a weaker aurophilic contact than **4**, displays the strongest Au–Tl interaction, with a Au–Tl distance of 2.8881(8) Å. The strongest metallophilic contacts are found in complex **4** [$d(\text{Au–Tl}) = 3.0360(4)$, $d(\text{Au–Au}) = 3.3294(6)$ Å], while compound **6** displays the longest Au–Tl distance of the three complexes [3.1483(4) Å]. In spite of these differences, all Au–Tl distances lie within the range of Au–Tl distances found in relevant structures: the distances vary from 2.804 Å in the metallocryptand [AuPdTl(P₂phen)₃][BF₄]₂·2.5CH₂Cl₂²³ to 3.4899(6) Å in the polymeric [Tl(1,10-phen)][Au(C₆F₅)₂]^{7b} (average Au–Tl distance 3.070 Å).

Again, the influence of the ligands bonded to thallium is revealed by the Tl–S distances found in the three complexes, since the structure of compound **4**, which contains the thioether [9]aneS₃, displays shorter Tl–S bond distances than **3** or **6**, in which the bulkier macrocycle [24]aneS₈ is present. Thus, the Tl–S bond lengths in **4** range from 3.0246(17) to 3.1154(19) Å, the longer one being of the same order as those described for [Tl([9]aneS₃)]PF₆^{16e} (from 3.092(3) to 3.114(3) Å within each molecule), which contains the same ligand. In contrast, complexes **3** and **6** show weaker interactions between the thallium centres and the sulphur atoms of the thioether [24]aneS₈, displaying Tl–S distances between 3.256(7) and 3.587(7) Å in **3** and between 3.201(2) and 3.418(3) Å in **6**, values that compare well with those found in the related complex [Tl([24]aneS₈)]PF₆^{16d} [3.2413(11)–3.4734(14) Å].

The stronger Tl–S interactions in **4** correspond well with the lower coordination number that would be expected for Tl(I) when [9]aneS₃ is employed as a ligand and, accordingly, only three Tl–S bonds are present in **4**, but three additional Tl⋯F contacts between 3.257(5) and 3.336(6) Å, as well as the metallophilic Au⋯Tl interaction of 3.0360(4) Å increase the coordination number to 7. The environment of thallium could be described as distorted pentagonal bipyramidal with Au and S(1) occupying the apical positions. In the case of complex **3**, where the octathia macrocycle [24]aneS₈ is employed, five Tl–S interactions of different strengths appear (see Table 2), and no significant Tl⋯F contact is observed: this results in a pyramidal pentagonal environment for thallium with the gold centre occupying the vertex of the pyramid. In contrast, in the crystal

structure of **6** a higher number of interactions is observed: thus, there are four weak Tl–S bonds [3.201(2)–3.418(3) Å] and two even weaker interactions [Tl–S(3)#2 = 3.500(3) and Tl–S(4) = 3.744(2) Å]. In addition, the Tl⋯Au contact of 3.1483(4) Å and two Tl⋯F interactions of 3.110(4) and 2.968(6) Å give rise to a more complex environment for thallium.

Photophysical properties

The absorption spectra of complexes **1–3** show similar features displaying two bands at 235 and 287 nm. The first one, which is also present in the precursor complex NBU₄[Au(C₆Cl₅)₂], is assigned to a $\pi \rightarrow \pi^*$ transition in the pentachlorophenyl rings. A similar assignment was previously made for related complexes.^{5c} The possibility of an $n \rightarrow \sigma^*$ transition in the thioether ligands cannot be ruled out since the energy of such transitions has been reported at similar energies²⁴ and the ligands show one absorption at 234 nm, although with less intensity. Therefore, it can be masked by the more intense $\pi \rightarrow \pi^*$ transition of the C₆Cl₅ ligands. In the case of the pentafluorophenyl derivatives **4–6**, the spectra are featureless, showing a broad band between 225 and 275 nm that is likely to contain the two peaks at 241 and 263 nm of the gold precursor NBU₄[Au(C₆F₅)₂].

As we expected, all the complexes display rich optical behaviour in the solid state. Thus, they display emissions between 445 nm and 526 nm at room temperature, and between 441 and 599 nm when the measurements are carried out at liquid nitrogen temperature (77 K) (see Table 5). In most cases the spectra show a single emission, but in the case of complexes **1** and **4** a low-intensity shoulder is evident at low temperature (see Fig. 4). By contrast, all the complexes display a single emission in butyronitrile glass at 77 K and none of them show luminescence in solution at room temperature. All these data seem to be related to the different structures of the complexes in the solid state, which depend on the sulphur donor ligand (see above), or on the different disposition that they adopt in the different media. For example, the fact that none of the complexes is luminescent in solution is likely to be related to the rupture of the metal–metal interactions

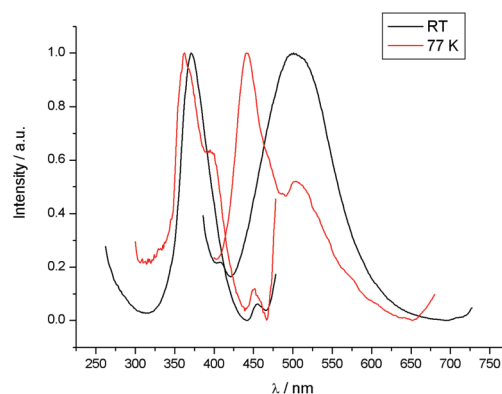


Fig. 4 Excitation and emission spectra for complex **4** in the solid state at RT and 77 K.

promoted by the solvent, which is compatible with the conductivity values found in all cases (see the Experimental section).

Therefore, the presence of intermetallic interactions in the solid state and their strength seem to be the key to explain the luminescence of these complexes. In the case of the emissions in butyronitrile glass at 77 K the values of energy are almost identical to those of the $[\{Au(C_6Cl_5)_2\}Tl]_n$ chains in the same solvent. Therefore, the butyronitrile molecules probably displace the sulphur donor ligands from the coordination sphere of thallium giving rise to the same species.

Another factor that should be considered is the disposition of the metal centres in the structures. In this sense, what is known from the X-ray diffraction studies is that two different structural dispositions are observed: that present in complex **4**, which shows a Tl–Au–Au–Tl unit, and those of complexes **3** and **6**, in which two Au–Tl moieties are connected by a [24]aneS₈ thioether ligand (see X-ray structures discussion).

In the case of complex **4**, its emission spectrum shows a broad band at 501 nm at room temperature and two bands at 77 K, one of high intensity placed at 441 nm and another one slightly shifted to the red (at 505 nm) of lower intensity (see Fig. 4). These bands are likely to arise from two connected excited states since both are obtained with the same excitation energy (363 nm). In this sense, the band placed at higher energy is assigned to arise from a metal–metal (gold) to ligand (π^* orbital from C₆F₅ rings) charge transfer (MMLCT) in the interacting $[Au(C_6F_5)_2]^-$ units, since the gold precursor NBu₄ $[Au(C_6F_5)_2]$ displays an emission at 433 nm at low temperature and it is not luminescent at room temperature. The slight shift of the emission in complex **4** can be attributed to the interaction between two of these units, which destabilize the HOMO and stabilize the LUMO reducing the HOMO–LUMO band gap.²⁵ On the other hand, the band that appears at lower energy is likely to arise from a ligand–metal ($[Au(C_6F_5)_2]^-$) to metal–metal (gold–thallium) charge transfer (LMMCT). In fact, a tetranuclear gold/thallium complex which displays a similar distribution of metals ($[Tl(bipy)]_2[Au(C_6F_5)_2]_2$) shows an emission at similar energy, which was attributed to this transition based on previous TD-DFT (Time Dependent-Density Functional Theory) calculations.^{7a}

In the case of the pentachlorophenyl complex **1** that contains the same sulphur donor ligand, the emission spectra also show a similar appearance, *i.e.*, one emission band at room temperature (525 nm) and an intense band at 471 nm and a shoulder at 512 nm at 77 K. In this case, the pentachlorophenylgold(i) precursor displays an emission at 514 nm at 77 K; therefore we assign this emission to a transition that arises from a metal–metal (gold) to ligand (π^* orbital from the C₆Cl₅ rings) charge transfer (MMLCT). By contrast, we assign the emission that appears at higher energy as arising from a ligand–metal ($[Au(C_6F_5)_2]^-$) to metal (thallium or gold–thallium) charge transfer transition (LMMCT). In this we can anticipate that the structure of this complex will show a longer Au–Tl distance, since the shorter the Au...Tl interaction is, the smaller the HOMO–LUMO gap is.^{9b,26} Therefore, taking into

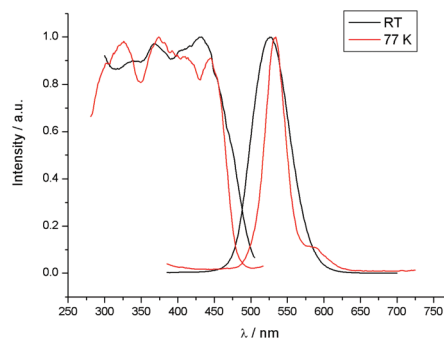


Fig. 5 Excitation and emission spectra for complex **3** in the solid state at RT and 77 K.

account the previous comments we can propose for complex **1** a structure similar to that found for complex **4**, but with a longer gold–thallium interaction.

In the case of complexes **3** and **6**, where both structures are known, a direct comparison can be made. Thus, both compounds are almost isostructural showing two $[\{Au(C_6Cl_5)_2\}Tl]$ moieties with each thallium interacting with five sulphur atoms of a common [24]aneS₈ ligand. Both of them show a single emission in their spectra at room temperature and at low temperature, showing a shift of the emission to the red at 77 K (see Table 5 and Fig. 5). In this case we can propose that the emission arises from a LMMCT (ligand (C₆X₅)–metal (gold) to metal (thallium) charge transfer) in the same way as those described above for complexes **1** and **4**. In this case the importance of the strength of the Au...Tl interaction is highlighted; since a shorter Au–Tl distance (2.89 Å) gives rise to a less energetic emission (526 nm) in **3**, while the more energetic emission in complex **6** (471 nm) corresponds to a longer Au–Tl distance (3.15 Å). Similarly, the shift to higher energy of the emissions at room temperature when compared to the corresponding low temperature measurements in both spectra is a consequence of the thermal expansion that larger gold–thallium distances and larger HOMO–LUMO gaps provoke.

For complexes **2** and **5** bearing the macrocycle [14]aneS₄, both spectra present a single asymmetric emission, whose shape could mask a second emission, as observed in the spectra of **1** and **4**. Nevertheless, in the case of complex **2**, this asymmetry disappears at low temperature, shifting the emission to the red (from 507 to 599 nm), while for complex **5** the asymmetry remains at low temperature and, as well as the main peak, is shifted to the red (see ESI†). Both observations clearly differ from what is seen for complexes **1** and **4**, so their solid state structures should be somehow different. Accordingly, we tentatively propose a similar Tl–Au–Au–Tl disposition of metals, but with a different environment for the thallium centres, since the ligands in **2** and **5** contain a fourth sulphur atom that can also bind this metal centres. In addition, the molar conductivity measurements for complexes **2** and **5** show values typical of 1:1 electrolytes (see the Experimental section); this is in accordance with the proposed structure. Note that such a slight difference could be significant enough

to modify the optical properties of these compounds. In fact, as mentioned in the introduction, in previous papers we have described some examples of Au/Tl complexes in which the luminescent properties are determined by the structural disposition and the Tl(I) environment.⁷

Finally, if we observe the data of all the complexes we can establish some interesting trends when we compare similar structures or S-donor ligands: (1) Complexes with C₆F₅ groups give shorter lifetime values than C₆Cl₅ complexes. (2) Complexes with C₆F₅ groups emit at shorter wavelengths than the corresponding C₆Cl₅ ones. (3) The quantum yields in the solid state are higher in the case of the C₆Cl₅ complexes. All of these characteristics can be incorporated into design strategies that permit the rational synthesis of complexes for practical applications.

DFT calculations

The rich structure-dependent emissive properties of complexes 1–6 in the solid state prompted us to study from a theoretical point of view the origin of the electronic transitions responsible for this behaviour. We have therefore carried out DFT and TD-DFT calculations on representative model systems of complexes 3, 4 and 6 (models 3a, 4a and 6a, respectively) that display the two types of structural disposition determined for these Au(I)–Tl(I) systems with different ring size crown thioethers. Since theoretical models incorporating all the metalphilic interactions are too big for optimization runs, we have built up the model systems directly from the X-ray diffraction data. Model 4a represents the uncommon Tl–Au–Au–Tl discrete disposition found in the corresponding structure of complex 4; meanwhile, models 3a and 6a represent the metalphilic Au⋯Au and Au⋯Tl interactions in a model system that leaves the [24]aneS₈ thioether ligand only coordinated to one Tl(I) center (see Fig. 6). These tetranuclear models 3a and 6a consist of the molecular fragments that contain the repeat unit of the polymeric complex 3 displaying all the interactions present in the solid state.

A study of the molecular orbitals (MOs) along with a population analysis was used to check the contribution of each atom to each occupied orbital for model 4a (see Table 6). The population analysis of the highest occupied MOs shows that while the HOMO orbital is mainly located at the [Au(C₆F₅)₂][−] units (79%) with a small contribution from the Tl(I) centres (14), from HOMO – 1 to HOMO – 4 a clear main contribution

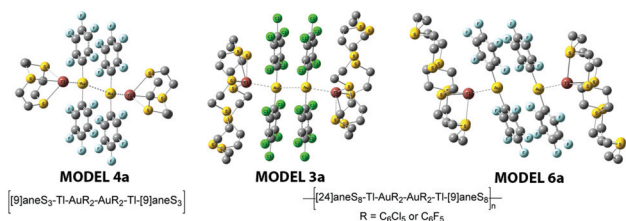


Fig. 6 Theoretical model systems [Au₂(C₆F₅)₄Tl₂([9]ane-S₃)₂] (4a) (left), [Au₂(C₆Cl₅)₄Tl₂([24]ane-S₈)₂] (3a) (center) and [Au₂(C₆F₅)₄Tl₂([24]ane-S₈)₂] (6a) (right).

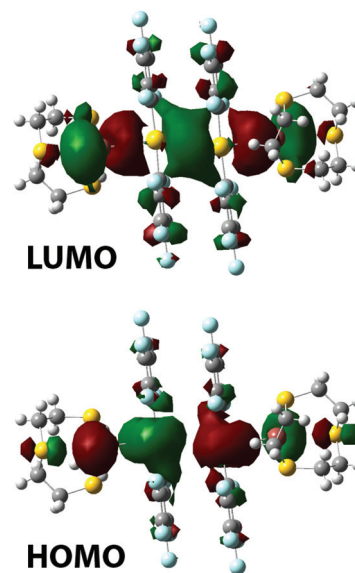


Fig. 7 Frontier molecular orbitals HOMO and LUMO for model system 4a.

from the C₆F₅ ligands is found. On the other hand, the population analysis of the lowest empty orbitals shows a main contribution from the Tl(I) centres to the LUMO orbital (43%), but also from the [Au(C₆F₅)₂][−] units (50%) and a main contribution from the Tl(I) centres (>80%) to the LUMO + 1 and LUMO + 2 orbitals. In view of these results the lowest electronic transitions should be of the charge transfer type since a clear difference in the composition of the highest occupied MOs and the lowest empty ones is observed. The shape of the orbitals is shown in Fig. 7.

The first ten excitation energies of models 4a have been calculated at the TD-DFT level of theory as described in the computational methods section. We have carried out an analysis of the energy, strength, and orbitals involved in the first singlet–singlet excitations, which reproduce the vertical electronic excitations that could be related with the luminescent behaviour observed for complex 4. The results are depicted in Table 7. Among the first 10 singlet–singlet excitations the ones giving the highest oscillator strengths, *i.e.*, excitations 1, 3 and 7, are studied in detail. Thus, the lowest theoretical singlet–singlet excitation appears at 323 nm (experimental excitation at 363 nm at 77 K) and displays a large oscillator strength value. This excitation consists of an electronic transition between HOMO and LUMO MOs and, as we have commented above, it can be considered as a charge transfer from the interacting [Au(C₆F₅)₂][−]⋯[Au(C₆F₅)₂][−] units that mainly contribute to the HOMO (79%), to the Tl⋯Au interacting metals that mainly contribute to the LUMO orbital (71%), with some participation from the C₆F₅ ligands (22%). This transition can be assigned to the one observed experimentally that is responsible for the low energy emission of complex 4 at 77 K (experimental emission at 505 nm). If we analyze the 3rd and 7th theoretical singlet–singlet excitations that appear at 302 and 296 nm, we observe a slight difference with the first one that is a different origin of electronic excitation. The starting orbitals in both

cases (HOMO – 2 and HOMO – 4) are mainly located at the anionic $C_6F_5^-$ ligands of the interacting $[Au(C_6F_5)_2]^- \cdots [Au(C_6F_5)_2]^-$ units, while the arriving orbital is the same as in the first singlet–singlet excitation, *i.e.*, the LUMO orbital. In view of these results we can state that the vertical excitations of singlet parentage mainly arrive into the lowest empty orbital LUMO. However, the experimental observation of a high-energy emission at 441 nm assigned to a metal–metal (gold) to ligand (π^* orbital from C_6F_5 rings) charge transfer (MMLCT) is not easy to assign from the calculation of the vertical excitation from the ground state (TD-DFT approach). The fact that two emissions appear by excitation at the same energy and change their relative intensities with temperature seems to indicate the presence of two interconnected singlet excited states (experimental lifetimes for the emissions at 77 K are in the nanosecond range). It seems likely that upon vertical excitation the molecular excited state structure could be relaxed towards two different local minima from which the emissions would occur, depending on the temperature. The different structural distortions would be explained by the full optimization of both excited states but, unfortunately, the large size of the theoretical models precludes these calculations. Therefore, although the assignment of the high energy emission is reasonable from an experimental viewpoint it cannot be evaluated at this stage from a theoretical one, due to a very large computational cost.

The second part of the theoretical study has been focused on the analysis of the electronic excitations observed in the Au–Tl complexes bearing the [24]aneS₈ thioether ligand. As has been shown in the structural studies section, both complexes $\{[Au(C_6Cl_5)_2]_2Tl_2([24]aneS_8)\}_n$ (**3**) and $\{[Au(C_6F_5)_2]_2Tl_2([24]aneS_8)\}$ (**6**) display analogous structures with the exception of different perhalophenyl ligands, C_6Cl_5 (**3**) and C_6F_5 (**6**) and the presence of aurophilic interactions in **3** that are absent in **6** and result in a polymer chain or a discrete tetranuclear molecule, respectively. The study of the electronic structure and population analysis of model systems **3a** and **6a** shows significant differences that could be attributed to the main difference between both complexes (Table 6 and Fig. 8), that is, the presence of much shorter intermetallic distances in the case of complex **3** than the ones observed in complex **6**.

Thus, in the case of model **3a** the frontier orbitals HOMO and LUMO are mostly located at the $[Au(C_6F_5)_2]^-$ units and the Tl(I) centres, the next occupied MOs (H – 1, H – 8 to H – 11), are mostly ligand-based. This trend is in agreement with short intermetallic distances that are directly related to a reduction of the metal-based HOMO–LUMO gap. In the case of model **6a**, the presence of larger intermetallic distances changes the HOMO, which is now placed at the thioether ligand, with HOMO – 2 and LUMO now associated with the aurate-thallium based MOs (see Table 6). Nevertheless, although the population analysis of the frontier orbitals shows some differences between these complexes, the lowest singlet–singlet theoretical excitations calculated at the TD-DFT level display a similar behaviour (Table 7). In the case of model **3a** the most intense theoretical excitation (among the first 10 excitations) is the first one (theoretical excitation at 387 nm, experimental continuum profile in the 300–450 nm) and consists of a vertical excitation between HOMO and LUMO orbitals, that is, a charge transfer from the interacting $[Au(C_6F_5)_2]^- \cdots [Au(C_6F_5)_2]^-$ units that mainly contribute to the HOMO (67%), to the Tl–Au interacting metals that mainly contribute to the LUMO orbital (54%), with an important participation from the C_6Cl_5 ligands (42%) (Table 7). This result is similar to that obtained for model **4a** and explains the origin of the emission proposed experimentally for complex **3**. If we analyze the singlet–singlet electronic excitations calculated for model **6a** we observe now that the main excitation is the first one (theoretical excitation at 298 nm, experimental maximum at 358 nm) and it consists of a mixed electronic transition mainly involving aurate-thallium-based HOMO – 2 and LUMO MOs with the contribution of a HOMO–LUMO transition (Table 7). In view of the character of the involved orbitals we propose that when the intermetallic distances are longer the main electronic singlet–singlet excitation is still a charge transfer between the aurate units that mainly contribute to the HOMO – 2 (61%), and the Tl–Au interacting metals (60%), although a ligand ([24]aneS₈) to metal–metal (gold–thallium) charge transfer transition contribution cannot be excluded. The relationship between the larger intermetallic distances and the different contributions to the origin of the emissive behaviour for models **3a** and **6a** would explain the different emission energies found for complexes **3** and **6**.

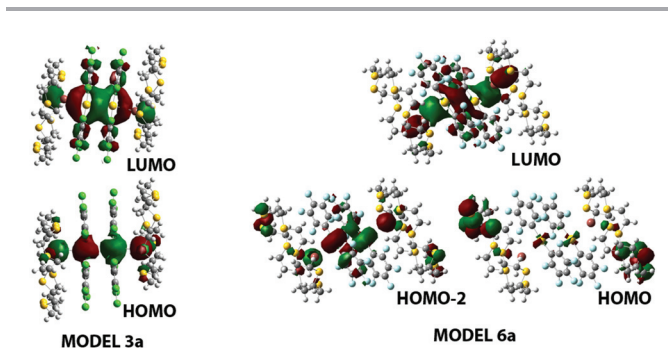


Fig. 8 Frontier molecular orbitals and HOMO and LUMO for model systems **3a** and **6a**.

Conclusions

The use of crown thioethers (L) against $[Au(C_6X_5)_2]Tl$ affords compounds of stoichiometries $[Au(C_6X_5)_2]Tl(L)_2$ or $[Au(C_6F_5)_2]_2Tl_2(L)$ depending on the size of the macrocycle, which can act as a terminal or as a bridging S-donor ligand. The formation of Tl–S bonds and Au–Tl or Au–Tl and Au–Au contacts leads to unusual structures for Au/Tl complexes with polymeric $[-L-Tl-Au-Au-Tl-]_n$ (**3**) or tetranuclear $[L-Tl-Au-Au-Tl-L]$ (**4**) or Au–Tl–L–Tl–Au (**6**) dispositions, clearly influenced by the nature of the ligands at the metal centres.

The metal–metal interactions are the origin of the luminescence observed for all the complexes in the solid state, a

property that strongly depends on the halogens present in the aryl groups: fluorinated compounds display shorter lifetimes and emission wavelengths, as well as lower quantum yields than the chlorinated ones.

DFT calculations on representative model systems of some of the complexes also agree with the assignment of the origin of their optical properties and show a good correlation between the intermetallic distances and emission energies.

Experimental

General

Thioether crown ligands,²⁷ $[\{\text{Au}(\text{C}_6\text{Cl}_5)_2\}\text{Tl}]_n$ ^{5b} and $[\{\text{Au}(\text{C}_6\text{F}_5)_2\}\text{Tl}]_n$ ^{10a} were prepared according to the literature.

Instrumentation

Infrared spectra were recorded in the 4000–200 cm⁻¹ range on a Nicolet Nexus FT-IR using Nujol mulls between polyethylene sheets. C, H and S analyses were carried out with a Perkin-Elmer 240C microanalyzer. Molar conductivities were measured in *ca.* 5 × 10⁻⁴ M acetone solutions with a Jenway 4510 conductivity meter. Mass spectra were recorded with a Bruker Microflex MALDI-TOF using dithranol (DIT) or 11-dicyano-4-*tert*-butylphenyl-3-methylbutadiene (DCTB) as the matrix. ¹H and ¹⁹F NMR spectra were recorded with a Bruker Avance 400 in [D₈]tetrahydrofuran. Chemical shifts are quoted relative to SiMe₄ (¹H, external) and CFCl₃ (¹⁹F, external). Excitation and emission spectra in the solid state were recorded with a Jobin-Yvon Horiba Fluorolog 3–22 Tau-3 spectrofluorimeter. Lifetime measurements were recorded with a DataStation HUB-B with a nanoLED controller and DAS6 software. The nanoLED employed for lifetime measurements was one of 370 nm with pulse lengths of 0.8–1.4 ns. The lifetime data were fitted with the Jobin-Yvon software package. Measurements at 77 K were done with an Oxford Cryostat Optistat DN with an accessory for solid samples.

Synthesis

$[\{\text{Au}(\text{C}_6\text{Cl}_5)_2\}\text{Tl}(\text{[9]aneS}_3)]_2$ (1). To a well stirred solution of $[\{\text{Au}(\text{C}_6\text{Cl}_5)_2\}\text{Tl}]_n$ (100 mg, 0.111 mmol) in tetrahydrofuran, [9]aneS₃ (20 mg, 0.111 mmol) was added. The mixture was stirred at room temperature for 3 h, and then the solvent was partially removed under reduced pressure and, finally, the addition of *n*-hexane led to the precipitation of product 1 as a yellow solid that was filtered and washed with *n*-hexane (86.4 mg, 72% yield). Elemental analysis (%) calcd for C₁₈H₁₂AuCl₁₀S₃Tl (1080.36): C 22.01, H 1.12, S 8.90. Found: C 22.71, H 1.20, S 8.90. Λ_M : 117 Ω⁻¹ cm² mol⁻¹. ¹H NMR (400 MHz, [D₈]tetrahydrofuran, ppm): δ 3.20 ppm (s, 12 H, CH₂). MALDI-TOF(–) *m/z* (%): 695 [Au(C₆Cl₅)₂][–] (100), 1595 $[\{\text{Au}(\text{C}_6\text{Cl}_5)_2\}\text{Tl}]^–$ (9). MALDI-TOF(+) *m/z* (%): 385 $[\text{Tl}(\text{[9]aneS}_3)]^+$ (100). FTIR (Nujol): ν ([Au(C₆Cl₅)₂][–]) at 834 and 617 cm⁻¹.

$[\{\text{Au}(\text{C}_6\text{Cl}_5)_2\}\text{Tl}(\text{[14]aneS}_4)]_2$ (2). [14]aneS₄ (30 mg, 0.111 mmol) was added to a solution of $[\{\text{Au}(\text{C}_6\text{Cl}_5)_2\}\text{Tl}]_n$ (100 mg, 0.111 mmol) in tetrahydrofuran. After 3 h of stirring, the

solution was concentrated under vacuum. Finally, the addition of *n*-hexane led to the precipitation of product 2 as a yellow solid that was filtered and washed with *n*-hexane (98.2 mg, 76% yield). Elemental analysis (%) calcd for C₂₂H₂₀AuCl₁₀S₄Tl (1168.53): C 22.61, H 1.73, S 10.98. Found: C 22.34, H 1.73, S 9.70. Λ_M : 117 Ω⁻¹ cm² mol⁻¹. ¹H NMR (400 MHz, [D₈]tetrahydrofuran, ppm): δ 2.01 (q, 4H, S–CH₂–CH₂–CH₂–S, ³J_{(H–H)} = 2 Hz), 2.73 (t, 8H, S–CH₂–CH₂–CH₂–S, ³J_{(H–H)} = 2 Hz), 2.85 (s, 8H, S–CH₂–CH₂–S). MALDI-TOF(–) *m/z* (%): 695 [Au(C₆Cl₅)₂][–] (100), 1595 $[\{\text{Au}(\text{C}_6\text{Cl}_5)_2\}\text{Tl}]^–$ (16). MALDI-TOF(+) *m/z* (%): 473 $[\text{Tl}(\text{[14]aneS}_4)]^+$ (100). FTIR (Nujol): ν ([Au(C₆Cl₅)₂][–]) at 837 and 614 cm⁻¹.}}

$[\{\text{Au}(\text{C}_6\text{Cl}_5)_2\}\text{Tl}_2(\text{[24]aneS}_8)]_n$ (3). To a well stirred solution of $[\{\text{Au}(\text{C}_6\text{Cl}_5)_2\}\text{Tl}]_n$ (85 mg, 0.095 mmol) in tetrahydrofuran, [24]aneS₈ (23 mg, 0.047 mmol) was added. The mixture was stirred at room temperature for 3 h, and then the solvent was partially removed under reduced pressure and, finally, the addition of *n*-hexane led to the precipitation of product 3 as a green solid that was filtered and washed with *n*-hexane (93.4 mg, 87% yield). Elemental analysis (%) calcd for C₄₀H₃₂Au₂Cl₂₀S₈Tl₂ (2279.27): C 21.13, H 1.42, S 11.26. Found C 21.10, H 1.52, S 11.96. Λ_M : 220 Ω⁻¹ cm² mol⁻¹. ¹H NMR (400 MHz, [D₈]tetrahydrofuran, ppm): δ 2.92 (s, 32H, CH₂). MALDI-TOF(–) *m/z* (%): 695 [Au(C₆Cl₅)₂][–] (100), 1595 $[\{\text{Au}(\text{C}_6\text{Cl}_5)_2\}\text{Tl}]^–$ (14). MALDI-TOF(+) *m/z* (%): 685 $[\text{Tl}(\text{[24]aneS}_8)]^+$ (66). FTIR (Nujol): ν ([Au(C₆Cl₅)₂][–]) at 834 and 614 cm⁻¹.

$[\{\text{Au}(\text{C}_6\text{F}_5)_2\}\text{Tl}(\text{[9]aneS}_3)]_2$ (4). [9]aneS₃ (24.5 mg, 0.136 mmol) was added to a suspension of $[\{\text{Au}(\text{C}_6\text{F}_5)_2\}\text{Tl}]_n$ (100 mg, 0.136 mmol) in toluene. After 2 h of stirring, the solution was concentrated under vacuum. Finally, the addition of *n*-hexane led to the precipitation of product 4 as a white solid that was filtered and washed with *n*-hexane (74.5 mg, 60% yield). Elemental analysis (%) calcd for C₁₈H₁₂AuF₁₀S₃Tl (915.82): C 23.61, H 1.32, S 10.50. Found C 24.73, H 1.88, S 10.44. Λ_M : 133 Ω⁻¹ cm² mol⁻¹. ¹H NMR (400 MHz, [D₈]tetrahydrofuran, ppm): δ 3.21 (s, 12 H, CH₂). ¹⁹F NMR (400 MHz, [D₈]tetrahydrofuran, ppm): δ –112.0 (m, 2F, F_o), –159.8 (t, 1F, F_p, ³J_{(F_p–F_m)} = 19.3 Hz), –161.3 (m, 2F, F_m). (MALDI-TOF(–) *m/z* (%): 531 [Au(C₆F₅)₂][–] (100), 1267 $[\{\text{Au}(\text{C}_6\text{F}_5)_2\}\text{Tl}]^–$ (20). MALDI-TOF(+) *m/z* (%): 385 $[\text{Tl}(\text{[9]aneS}_3)]^+$ (15). FTIR (Nujol): ν ([Au(C₆F₅)₂][–]) at 1502, 952 and 785 cm⁻¹.}

$[\{\text{Au}(\text{C}_6\text{F}_5)_2\}\text{Tl}(\text{[14]aneS}_4)]_2$ (5). [14]aneS₄ (36.5 mg, 0.136 mmol) was added to a suspension of $[\{\text{Au}(\text{C}_6\text{F}_5)_2\}\text{Tl}]_n$ (100 mg, 0.136 mmol) in toluene. After 2 h of stirring, the solution was concentrated under vacuum. Finally, the addition of *n*-hexane led to the precipitation of product 5 as a white solid that was filtered and washed with *n*-hexane (120 mg, 88% yield). Elemental analysis (%) calcd for C₂₂H₂₀AuF₁₀S₄Tl (1003.99): C 26.32, H 2.01, S 12.78. Found C 27.62, H 2.70, S 11.52. Λ_M : 108 Ω⁻¹ cm² mol⁻¹. ¹H NMR (400 MHz, [D₈]tetrahydrofuran, ppm): δ 2.01 (q, 4H, S–CH₂–CH₂–CH₂–S, ³J_{(H–H)} = 2 Hz), 2.73 (t, 8H, S–CH₂–CH₂–CH₂–S, ³J_{(H–H)} = 2 Hz), 2.85 (s, 8H, S–CH₂–CH₂–S). ¹⁹F NMR (400 MHz, [D₈]tetrahydrofuran, ppm): δ –112.0 (m, 2F, F_o), –159.9 (t, 1F, F_p, ³J_{(F_p–F_m)} = 19.8 Hz), –161.4 (m, 2F, F_m). MALDI-TOF(–) *m/z* (%): 531 [Au(C₆F₅)₂][–]}}}

Table 1 Data collection and structure refinement details for 1–3

Compound	3	4	6
Chemical formula	C ₄₀ H ₃₂ Au ₂ Cl ₂₀ S ₈ Tl ₂	C ₃₆ H ₂₄ Au ₂ F ₂₀ S ₆ Tl ₂	C ₄₀ H ₃₂ Au ₂ F ₂₀ S ₈ Tl ₂
Crystal habit	Green plate	Colourless block	Pale yellow plate
Crystal size/mm	0.14 × 0.09 × 0.03	0.45 × 0.3 × 0.2	0.3 × 0.2 × 0.1
Crystal system	Triclinic	Monoclinic	Triclinic
Space group	<i>P</i> 1	<i>P</i> 2 ₁ / <i>c</i>	<i>P</i> 1
<i>a</i> /Å	10.6829(11)	10.9933(3)	9.0826(5)
<i>b</i> /Å	11.9086(10)	11.7372(4)	12.5273(7)
<i>c</i> /Å	14.4564(12)	17.4726(6)	12.9677(5)
<i>α</i> /°	66.786(8)	90	115.204(3)
<i>β</i> /°	78.615(8)	92.688(2)	98.272(3)
<i>γ</i> /°	66.326(9)	90	103.410(3)
<i>V</i> /Å ³	1546.3(2)	3058.51(19)	1248.28(11)
<i>Z</i>	1	2	1
<i>D_c</i> /g cm ⁻³	2.449	2.701	2.596
<i>M</i>	2280.80	1831.58	1951.81
<i>F</i> (000)	1060	1672	900
<i>T</i> /°C	22	-100	-80
2θmax/°	50	55	55
μ(Mo-Kα)/mm ⁻¹	11.091	14.019	12.735
No. of refl. measured	8439	29 515	19 740
No. of unique refl.	5438	5174	5679
<i>R</i> _{int}	0.031	0.0803	0.0601
<i>R</i> [<i>F</i> > 2σ(<i>F</i>)] ^a	0.0516	0.0402	0.0389
<i>W</i> <i>r</i> [<i>F</i> ² , all refl.] ^b	0.136	0.1090	0.1068
No. of refl. used [<i>F</i> > 2σ(<i>F</i>)]	4340	4437	4564
No. of parameters	322	299	352
No. of restraints	309	97	125
<i>S</i> ^c	1.02	1.097	1.033
Max. residual electron density/e Å ⁻³	1.98	1.562	1.506

^a $R(F) = \sum ||F_o| - |F_c|| / \sum |F_o|$. ^b $wR(F^2) = [\sum \{w(F_o^2 - F_c^2)^2\} / \sum \{w(F_o^2)^2\}]^{0.5}$; $w^{-1} = \sigma^2(F_o^2) + (aP)^2 + bP$, where $P = [F_o^2 + 2F_c^2]/3$ and *a* and *b* are constants adjusted by the program. ^c $S = [\sum \{w(F_o^2 - F_c^2)^2\} / (n - p)]^{0.5}$, where *n* is the number of data and *p* the number of parameters.

Table 2 Selected bond lengths [Å] and angles [°] for complex 3

Tl(1)–S(1)	3.327(7)	Au(1)–Tl(1)	2.8881(8)
Tl(1)–S(4)	3.319(6)	Au(1)–Au(1)#1	3.3497(11)
Tl(1)–S(7)	3.256(7)	Au(1)–C(20)	2.056(11)
Tl(1)–S(10)	3.366(6)	Au(2)–C(30)	2.046(12)
Tl(1)–S(1)#2	3.587(7)		
C(30)–Au(1)–C(20)	175.6(5)	Tl(1)–Au(1)–Au(1)#1	147.89(3)

Symmetry transformations used to generate equivalent atoms:
#1 -*x* + 1, -*y*, -*z* #2 -*x*, -*y* + 1, -*z*.

Table 3 Selected bond lengths [Å] and angles [°] for complex 4

Tl–S(1)	3.1154(19)	Tl–F(9)#3	3.285(5)
Tl–S(2)	3.0584(20)	Au–Tl	3.0360(4)
Tl–S(3)	3.0246(17)	Au–Au#1	3.3294(6)
Tl–F(2)#2	3.257(5)	Au–C(1)	2.056(7)
Tl–F(8)#3	3.336(6)	Au–C(11)	2.052(7)
C(11)–Au–C(1)	176.9(3)	Tl–Au–Au#1	158.410(14)

Symmetry transformations used to generate equivalent atoms:
#1 -*x* + 1, -*y* + 1, -*z* #2 -*x*, -*y* + 1, -*z* #3 -*x* + 1, -*y*, -*z*.

(100), 1267 [Au(C₆F₅)₂Tl]⁻ (24). MALDI-TOF(+) *m/z* (%): 473 [Tl([14]aneS₄)]⁺ (30). FTIR (Nujol): ν([Au(C₆F₅)₂Tl]⁻) at 1508, 955 and 785 cm⁻¹.

Table 4 Selected bond lengths [Å] and angles [°] for complex 6

Tl–S(1)	3.201(2)	Tl–F(10)	2.968(6)
Tl–S(2)	3.258(2)	Au–Tl	3.1483(4)
Tl–S(3)	3.418(3)	Au–C(1)	2.047(7)
Tl–S(4)#1	3.277(2)	Au–C(11)	2.046(7)
Tl–F(1)	3.110(4)		
C(11)–Au–C(1)	172.7(3)		

Symmetry transformations used to generate equivalent atoms:
#1 -*x* + 2, -*y* + 2, -*z* + 1.

[Au(C₆F₅)₂]₂Tl₂([24]aneS₈) (6). [24]aneS₈ (32.7 mg, 0.068 mmol) was added to a suspension of [Au(C₆F₅)₂Tl] (100 mg, 0.136 mmol) in toluene. After 2 h of stirring, the solution was concentrated under vacuum. Finally, the addition of *n*-hexane led to the precipitation of product 6 as a pale yellow solid that was filtered and washed with *n*-hexane (121 mg, 91% yield). Elemental analysis (%) calcd for C₄₀H₃₂Au₂F₂₀S₈Tl₂ (1951.87): C 24.60, H 1.65, S 13.14. Found C 23.52, H 1.64, S 13.83. Λ_M: 280 Ω⁻¹ cm² mol⁻¹. ¹H NMR (400 MHz, [D₈]tetrahydrofuran, ppm): δ 2.92 (s, 32 H, CH₂). ¹⁹F NMR (400 MHz, [D₈]tetrahydrofuran, ppm): δ -112.0 (m, 2F, F_o), -160.0 (t, 1F, F_p, ³J_(Fp-Fm) = 19.8 Hz), -161.5 (m, 2F, F_m). MALDI-TOF(-) *m/z* (%): 531 [Au(C₆F₅)₂Tl]⁻ (100), 1267

Table 5 Photophysical properties of complexes 1–6

	Solid (RT) em (exc)	Solid (77 K) em (exc)	Glass ^a (77 K) em (exc)	τ^b (ns)	Φ^b
$[\{\text{Au}(\text{C}_6\text{Cl}_5)_2\}\text{Tl}(\text{[9]aneS}_3)]_2$ (1)	525 (405)	471, 512 (sh) (360)	529 (362)	629.6	26
$[\{\text{Au}(\text{C}_6\text{Cl}_5)_2\}\text{Tl}(\text{[14]aneS}_4)]_2$ (2)	507 (369)	599 (369)	533 (370)	139.9	37
$[\{\text{Au}(\text{C}_6\text{Cl}_5)_2\}\text{Tl}(\text{[24]aneS}_8)]_n$ (3)	526 (433)	534 (374)	517 (363)	3069.2	89
NBu ₄ [Au(C ₆ Cl ₅) ₂] [Au(C ₆ Cl ₅) ₂] _n Tl _n		514 (369)	534 (370)		
$[\{\text{Au}(\text{C}_6\text{F}_5)_2\}\text{Tl}(\text{[9]aneS}_3)]_2$ (4)	501 (371)	441, 505 (sh) (363)	422 (296)	339.1	22
$[\{\text{Au}(\text{C}_6\text{F}_5)_2\}\text{Tl}(\text{[14]aneS}_4)]_2$ (5)	445, 507 (sh) (394)	460, 541 (sh) (379)	433 (292)	78.2	25
$[\{\text{Au}(\text{C}_6\text{F}_5)_2\}\text{Tl}_2(\text{[24]aneS}_8)]$ (6)	471 (372)	484 (358)	437 (271)	484.8	25
NBu ₄ [Au(C ₆ F ₅) ₂] [Au(C ₆ F ₅) ₂] _n Tl _n		433 (285)	431 (274)		

^a In butyronitrile (2×10^{-4} M). ^b Solid state at room temperature.

$[\{\text{Au}(\text{C}_6\text{F}_5)_2\}\text{Tl}]^-$ (18). MALDI-TOF(+) m/z (%): 685 $[\text{Tl}(\text{[24]aneS}_8)]^+$ (100). FTIR (Nujol): ν $[\{\text{Au}(\text{C}_6\text{F}_5)_2\}]^-$ at 1502, 953 and 779 cm^{-1} .

Crystallography

Crystals were mounted in inert oil on glass fibres and transferred into the cold gas stream of an Oxford Cryosystems open-flow cryostat mounted on a Nonius Kappa CCD diffractometer. Data were collected using graphite-monochromated Mo K α radiation ($\lambda = 0.71073$ Å). Scan type ω and ϕ . Absorption corrections: semiempirical (based on multiple scans). The structures were solved by direct methods and refined on F^2 using the program SHELXL97.²⁸ All non-hydrogen atoms were refined anisotropically with the exception of C8, C9, C11 and C12 in 3, and all hydrogen atoms were included using a riding model. Disorder of the C8, C9, C11 and C12 methylene groups of the macrocycle in 3 was modelled with occupancies of the two

alternative orientations refined to 0.53 and 0.47. In 6, S3, C23 and C24 are also disordered over two different positions with occupancies refined to 0.8 and 0.2. Further details of the data collection and refinement are given in Table 1. Selected bond lengths and angles are presented in Tables 2–4 and crystal structures of complexes 3, 4 and 6 are shown in Fig. 1–3.

Computational details

All calculations were carried out using the Gaussian09 program package.²⁹ DFT and time-dependent DFT calculations were carried out using the PBE functional.³⁰ The following basis set combinations were employed for the metals Au and

Table 6 Population analysis for model systems 3a, 4a and 6a. Contribution from each part of the molecule to the occupied orbitals (%)

Model	Orbital	Tl	Au	S-ligand	C ₆ X ₅
3a	LUMO	28	26	4	42
	HOMO	12	54	21	13
	HOMO(−1)	1	0	94	5
	HOMO(−8)	1	4	35	61
	HOMO(−9)	1	6	37	55
	HOMO(−10)	2	0	41	57
4a	HOMO(−11)	2	2	64	32
	LUMO(+2)	83	0	16	1
	LUMO(+1)	81	0	17	2
	LUMO	43	28	7	22
6a	HOMO	14	54	7	25
	HOMO(−1)	0	11	0	88
	HOMO(−2)	0	2	1	98
	HOMO(−3)	0	2	1	98
	HOMO(−4)	0	15	1	84
	LUMO(+2)	74	0	17	9
	LUMO(+1)	70	2	24	4
	LUMO	34	26	14	26
	HOMO	2	6	88	4
	HOMO(−2)	7	36	32	25
6a	HOMO(−3)	6	13	72	10
	HOMO(−4)	0	4	76	20
	HOMO(−5)	4	20	28	48

Table 7 TD-DFT first singlet excitation calculation for model systems 3a, 4a and 6a. Only excitations with larger oscillator strengths are included among the first 10 excitation calculations

Model	Exc.	λ_{calc} (nm)	f (s) ^a	Contributions ^b
3a	1	386.7	0.5874	HOMO → LUMO (100)
	9	303.7	0.0236	HOMO(−11) → LUMO (44.2) HOMO(−9) → LUMO (55.8)
	10	303.2	0.1358	HOMO(−11) → LUMO (13.0) HOMO(−10) → LUMO (61.5) HOMO(−9) → LUMO (11.8) HOMO(−8) → LUMO (11.3)
4a	1	323.5	0.8299	HOMO → LUMO (100)
	3	302.5	0.0414	HOMO(−2) → LUMO (100)
	7	295.8	0.2048	HOMO(−4) → LUMO (93.6) HOMO → LUMO(+2) (6.4)
6a	8	285.5	0.0019	HOMO(−1) → LUMO(+1) (81) HOMO(−4) → LUMO(+2) (12)
	1	298.2	0.4651	HOMO(−2) → LUMO (65.4) HOMO → LUMO (31.9)
	6	278.2	0.1903	HOMO(−5) → LUMO (27.4) HOMO(−2) → LUMO(+2) (16.2) HOMO → LUMO (14.0)
	7	277.5	0.0712	HOMO(−3) → LUMO(+1) (11.9) HOMO → LUMO(+1) (11.2) HOMO(−11) → LUMO (13.0) HOMO(−10) → LUMO (61.5) HOMO(−9) → LUMO (11.8) HOMO(−8) → LUMO (11.3)

^a Oscillator strength (f) shows the mixed representation of both velocity and length representations. ^b Value is $|\text{coeff}|^2 \times 100$.

Tl: the 19-VE and 21-VE pseudo-potentials from Stuttgart and the corresponding basis sets augmented with two f polarization functions were used,³¹ respectively. The rest of the atoms were treated with SVP basis sets.^{32,33}

Acknowledgements

D.G.I.(MEC)/FEDER (project number CTQ2010-20500-C02-02) and MIUR (project PRIN 2009–2009Z9ASCA) are acknowledged for financial support.

Notes and references

- (a) R. Hoffmann, *Angew. Chem., Int. Ed. Engl.*, 1987, **26**, 846; (b) J. M. Williams, A. J. Schultz, A. E. Underhill and K. Carneiro, in *Extended Linear Chain Compounds*, Plenum Press, New York, vol. 1–3, 1982.
- (a) H. Schmidbaur, in *Gold: Progress in Chemistry, Biochemistry and Technology*, John Wiley & Sons, New York, 1999; (b) H. Schmidbaur, *Nature*, 2001, **413**, 31; (c) H. Schmidbaur, *Gold Bull.*, 1990, **23**, 11; (d) H. Schmidbaur, *Gold Bull.*, 2000, **33**, 3; (e) F. Scherbaum, A. Grömann, B. Huber, C. Krüger and H. Schmidbaur, *Angew. Chem., Int. Ed. Engl.*, 1988, **27**, 1544; (f) F. Scherbaum, A. Grömann, G. Müller and H. Schmidbaur, *Angew. Chem., Int. Ed. Engl.*, 1989, **28**, 463; (g) H. Schmidbaur, F. Scherbaum, B. Hubert and G. Müller, *Angew. Chem., Int. Ed. Engl.*, 1988, **27**, 419.
- (a) P. Pyykkö, *Chem. Rev.*, 1997, **97**, 597; (b) P. Pyykkö, *Angew. Chem., Int. Ed.*, 2004, **43**, 4412; (c) P. Pyykkö, *Inorg. Chim. Acta*, 2005, **358**, 4113; (d) P. Pyykkö, *Chem. Soc. Rev.*, 2008, **37**, 1967.
- (a) J. M. Forward, J. P. Fackler Jr. and Z. Assefa, in *Optoelectronic Properties of Inorganic Compounds*, ed. D. M. Roundhill and J. P. Fackler Jr., Plenum, New York, 1999, pp. 195–226; (b) J. M. López-de-Luzuriaga, in *Modern Supramolecular Gold Chemistry*, ed. A. Laguna. Wiley-VCH, Weinheim, 2008, p. 347; (c) E. J. Fernández, A. Laguna and J. M. López-de-Luzuriaga, *Gold Bull.*, 2001, **34**, 14, and references therein.
- (a) E. J. Fernández, A. Laguna, J. M. López-de-Luzuriaga and M. Monge, *Spanish Patent*, P200001391, 2003; (b) E. J. Fernández, J. M. López-de-Luzuriaga, M. Monge, M. E. Olmos, J. Pérez, A. Laguna, A. A. Mohammed and J. P. Fackler Jr., *J. Am. Chem. Soc.*, 2003, **125**, 2022; (c) E. J. Fernández, J. M. López-de-Luzuriaga, M. Monge, M. Montiel, M. E. Olmos, J. Pérez, A. Laguna, F. Mendizábal, A. A. Mohamed and J. P. Fackler Jr., *Inorg. Chem.*, 2004, **43**, 3573; (d) E. J. Fernández, J. M. López-de-Luzuriaga, M. Monge, M. E. Olmos, R. C. Puelles, A. Laguna, A. A. Mohamed and J. P. Fackler Jr., *Inorg. Chem.*, 2008, **47**, 8069.
- See for example: (a) E. J. Fernández, A. Garau, A. Laguna, T. Lasanta, V. Lippolis, J. M. López-de-Luzuriaga, M. Montiel and M. E. Olmos, *Organometallics*, 2010, **29**, 2951; (b) E. J. Fernández, A. Laguna, T. Lasanta, J. M. López-de-Luzuriaga, M. Montiel and M. E. Olmos, *Inorg. Chim. Acta*, 2010, **363**, 1965.
- (a) E. J. Fernández, P. G. Jones, A. Laguna, J. M. López-de-Luzuriaga, M. Monge, J. Pérez and M. E. Olmos, *Inorg. Chem.*, 2002, **41**, 1056; (b) E. J. Fernández, P. G. Jones, A. Laguna, J. M. López-de-Luzuriaga, M. Monge, M. Montiel, M. E. Olmos and J. Pérez, *Z. Naturforsch., B: Chem. Sci.*, 2004, **59**, 1379; (c) E. J. Fernández, A. Laguna, J. M. López-de-Luzuriaga, M. Montiel, M. E. Olmos and J. Pérez, *Organometallics*, 2005, **24**, 1631.
- (a) M. F. Hawthorne and Z. Zheng, *Acc. Chem. Res.*, 1997, **30**, 267; (b) M. F. Hawthorne, *Pure Appl. Chem.*, 1994, **66**, 245; (c) J. D. Wuest, *Acc. Chem. Res.*, 1999, **32**, 81; (d) J. Vaugois, M. Simard and J. D. Wuest, *Coord. Chem. Rev.*, 1995, **95**, 55.
- (a) T. Lasanta, M. E. Olmos, A. Laguna, J. M. López-de-Luzuriaga and P. Naumov, *J. Am. Chem. Soc.*, 2011, **133**, 16358; (b) A. Laguna, T. Lasanta, J. M. López-de-Luzuriaga, M. Monge, P. Naumov and M. E. Olmos, *J. Am. Chem. Soc.*, 2010, **132**, 456; (c) E. J. Fernández, A. Laguna, J. M. López-de-Luzuriaga, M. E. Olmos and R. C. Puelles, *Z. Naturforsch., B: Chem. Sci.*, 2009, **64**, 1500; (d) E. J. Fernández, J. M. López-de-Luzuriaga, M. Monge, M. E. Olmos, R. C. Puelles, A. Laguna, A. A. Mohamed and J. P. Fackler Jr., *Inorg. Chem.*, 2008, **47**, 8069.
- (a) E. J. Fernández, A. Laguna, J. M. López-de-Luzuriaga, M. Monge, M. Montiel, M. E. Olmos and J. Pérez, *Organometallics*, 2004, **23**, 774; (b) E. J. Fernández, A. Laguna, T. Lasanta, J. M. López-de-Luzuriaga, M. Montiel and M. E. Olmos, *Organometallics*, 2008, **27**, 2971.
- (a) E. J. Fernández, J. M. López-de-Luzuriaga, M. Monge, M. E. Olmos, J. Pérez and A. Laguna, *J. Am. Chem. Soc.*, 2002, **124**, 5942; (b) E. J. Fernández, J. M. López-de-Luzuriaga, M. E. Olmos, J. Pérez, A. Laguna and M. C. Lagunas, *Inorg. Chem.*, 2005, **44**, 6012.
- M. Arca, T. Aroz, M. C. Gimeno, M. Kulcsar, A. Laguna, T. Lasanta, V. Lippolis, J. M. López-de-Luzuriaga, M. Monge and M. E. Olmos, *Eur. J. Inorg. Chem.*, 2011, 2288.
- (a) S. Wang, J. P. Fackler Jr., C. King and J. C. Wang, *J. Am. Chem. Soc.*, 1988, **110**, 3308; (b) S. Wang, G. Garzón, C. King, J. C. Wang and J. P. Fackler Jr., *Inorg. Chem.*, 1989, **28**, 4623.
- See for example: (a) S. R. Cooper and S. C. Rawle, in *Bioinorganic Chemistry*, Springer-Verlag, Berlin, Heidelberg, 1990, vol. 72; (b) S. R. Cooper, *Acc. Chem. Res.*, 1988, **21**, 141; (c) A. J. Blake and M. Schröder, *Adv. Inorg. Chem.*, 1990, **35**, 1; (d) T. Adachi, M. D. Durrant, D. L. Hughes, C. J. Pickett, R. L. Richards, J. Talarmin and T. Yoshida, *J. Chem. Soc., Chem. Commun.*, 1992, 1464; (e) C. Landgrafe and W. S. Sheldrick, *J. Chem. Soc., Dalton Trans.*, 1996, 989; (f) R. D. Adams, S. B. Fallon, J. L. Perrin, J. A. Queisser and

- J. H. Yamamoto, *Chem. Ber.*, 1996, **129**, 313; (g) H.-J. Kim, J.-H. Lee, I.-H. Suh and Y. Do, *Inorg. Chem.*, 1995, **34**, 796.
- 15 J. L. Shaw, J. Wolowska, D. Collison, J. A. K. Howard, E. J. L. McInnes, J. McMaster, A. J. Blake, C. Wilson and M. Schröder, *J. Am. Chem. Soc.*, 2006, **128**, 13827.
- 16 (a) G. H. Robinson, H. Zhang and J. L. Atwood, *Organometallics*, 1987, **6**, 887; (b) K. George, M. Jura, W. Levason, M. E. Light, L. P. Ollivere and G. Reid, *Inorg. Chem.*, 2012, **51**, 2231; (c) C. Gurnani, M. Jura, W. Levason, R. Ratnani, G. Reid and M. Webster, *Dalton Trans.*, 2009, 1611; (d) A. J. Blake, D. Fenske, W.-S. Li, V. Lippolis and M. Schröder, *J. Chem. Soc., Dalton Trans.*, 1998, 3961; (e) A. J. Blake, J. A. Greig and M. Schröder, *J. Chem. Soc., Dalton Trans.*, 1991, 529; (f) F. Cheng, A. L. Hector, W. Levason, G. Reid, M. Webster and W. Zhang, *Chem. Commun.*, 2008, 5508; (g) G. R. Willey, A. Jarvis, J. Palin and W. Errington, *J. Chem. Soc., Dalton Trans.*, 1994, 255; (h) H.-J. Kuppers, K. Wieghardt, B. Nuber and J. Weiss, *Z. Anorg. Allg. Chem.*, 1989, **577**, 155; (i) G. R. Willey, M. T. Lakin, M. Ravindra and N. W. Alcock, *J. Chem. Soc., Chem. Commun.*, 1991, 271.
- 17 (a) Sanaullah, K. Kano, R. S. Glass and G. S. Wilson, *J. Am. Chem. Soc.*, 1993, **115**, 592; (b) E. Wyer, G. Giucardo, V. Leigh, H. Muller-Bunz and M. Albrecht, *J. Organomet. Chem.*, 2011, **696**, 2882; (c) A. J. Blake, N. R. Champness, S. M. Howdle and P. E. Webb, *Inorg. Chem.*, 2000, **39**, 1035; (d) D. Parker, P. S. Roy, G. Ferguson and M. M. Hunt, *Inorg. Chim. Acta*, 1989, **155**, 227; (e) W. N. Setzer, Q. Guo, G. J. Grant, J. L. Hubbard, R. S. Glass and D. G. VanDerveer, *Heteroat. Chem.*, 1990, **1**, 317; (f) M. L. Helm, L. L. Hill, J. P. Lee, D. G. VanDerveer and G. J. Grant, *Dalton Trans.*, 2006, 3534; (g) M. Wilhelm, S. Deeken, E. Berssen, W. Saak, A. Lutzen, R. Koch and H. Strasdeit, *Eur. J. Inorg. Chem.*, 2004, 2301.
- 18 A. J. Blake, J. A. Greig and M. Schröder, *J. Chem. Soc., Dalton Trans.*, 1992, 2987.
- 19 R. Usón, A. Laguna, M. Laguna, B. R. Manzano, P. G. Jones and G. M. Sheldrick, *J. Chem. Soc., Dalton Trans.*, 1984, 285.
- 20 R. Usón, A. Laguna, M. Laguna, B. R. Manzano and A. Tapia, *Inorg. Chim. Acta*, 1985, **101**, 151.
- 21 (a) E. J. Fernández, A. Laguna, J. M. López-de-Luzuriaga, M. E. Olmos and J. Pérez, *Dalton Trans.*, 2004, 1801; (b) O. Crespo, E. J. Fernández, P. G. Jones, A. Laguna, J. M. López-de-Luzuriaga, A. Mendía, M. Monge and M. E. Olmos, *Chem. Commun.*, 1998, 2233; (c) E. J. Fernández, A. Laguna, J. M. López-de-Luzuriaga, F. Mendizabal, M. Monge, M. E. Olmos and J. Pérez, *Chem.-Eur. J.*, 2003, **9**, 456; (d) E. J. Fernández, A. Laguna, J. M. López-de-Luzuriaga, M. Montiel, M. E. Olmos and J. Pérez, *Inorg. Chim. Acta*, 2005, **358**, 4293; (e) E. J. Fernández, A. Laguna, J. M. López-de-Luzuriaga, M. Montiel, M. E. Olmos and J. Pérez, *Organometallics*, 2006, **25**, 1689.
- 22 E. J. Fernández, A. Laguna, J. M. López-de-Luzuriaga, M. E. Olmos and J. Pérez, *Chem. Commun.*, 2003, 1760.
- 23 V. J. Catalano and M. A. Malwitz, *J. Am. Chem. Soc.*, 2004, **126**, 6560.
- 24 E. Pretsch, P. Bühlmann, C. Affolter, A. Herrera and R. Martínez, in *Structure Determination of Organic Compounds*, Springer-Verlag, Berlin, Heidelberg, New York, 2000.
- 25 E. J. Fernández, M. C. Gimeno, A. Laguna, J. M. López-de-Luzuriaga, M. Monge, P. Pyykkö and D. Sundholm, *J. Am. Chem. Soc.*, 2000, **122**, 7287.
- 26 E. J. Fernández, A. Laguna and J. M. López-de-Luzuriaga, *Dalton Trans.*, 2007, 1969.
- 27 (a) D. Sellmann and L. Zapf, *Angew. Chem.*, 1984, **96**, 799; (b) J. Buter and R. M. Kellog, *J. Org. Chem.*, 1981, **46**, 4481; (c) J. J. H. Edema, J. Buter and R. M. Kellog, *Tetrahedron*, 1991, **50**, 2095.
- 28 G. M. Sheldrick, *SHELXL97, Program for Crystal Structure Refinement*, University of Göttingen, Germany, 1997.
- 29 M. J. Frisch, G. W. Trucks, H. B. Schlegel, G. E. Scuseria, M. A. Robb, J. R. Cheeseman, G. Scalmani, V. Barone, B. Mennucci, G. A. Petersson, H. Nakatsuji, M. Caricato, X. Li, H. P. Hratchian, A. F. Izmaylov, J. Bloino, G. Zheng, J. L. Sonnenberg, M. Hada, M. Ehara, K. Toyota, R. Fukuda, J. Hasegawa, M. Ishida, T. Nakajima, Y. Honda, O. Kitao, H. Nakai, T. Vreven, J. A. Montgomery Jr., J. E. Peralta, F. Ogliaro, M. Bearpark, J. J. Heyd, E. Brothers, K. N. Kudin, V. N. Staroverov, R. Kobayashi, J. Normand, K. Raghavachari, A. Rendell, J. C. Burant, S. S. Iyengar, J. Tomasi, M. Cossi, N. Rega, N. J. Millam, M. Klene, J. E. Knox, J. B. Cross, V. Bakken, C. Adamo, J. Jaramillo, R. Gomperts, R. E. Stratmann, O. Yazyev, A. J. Austin, R. Cammi, C. Pomelli, J. W. Ochterski, R. L. Martin, K. Morokuma, V. G. Zakrzewski, G. A. Voth, P. Salvador, J. J. Dannenberg, S. Dapprich, A. D. Daniels, Ö. Farkas, J. B. Foresman, J. V. Ortiz, J. Cioslowski and D. J. Fox, *GAUSSIAN 09 (Revision A.1)*, Gaussian, Inc., Wallingford CT, 2009.
- 30 C. Adamo and V. Barone, *J. Chem. Phys.*, 1999, **110**, 6158.
- 31 D. Andrae, U. Haeussermann, M. Dolg, H. Stoll and H. Preuss, *Theor. Chim. Acta*, 1990, **77**, 123.
- 32 A. Schäfer, H. Horn and R. Ahlrichs, *J. Chem. Phys.*, 1992, **97**, 2571.
- 33 T. H. Dunning Jr., *J. Chem. Phys.*, 1994, **100**, 5829.